Supplementary Information

Supplementary Figure 1 – Regression of principle components against covariates

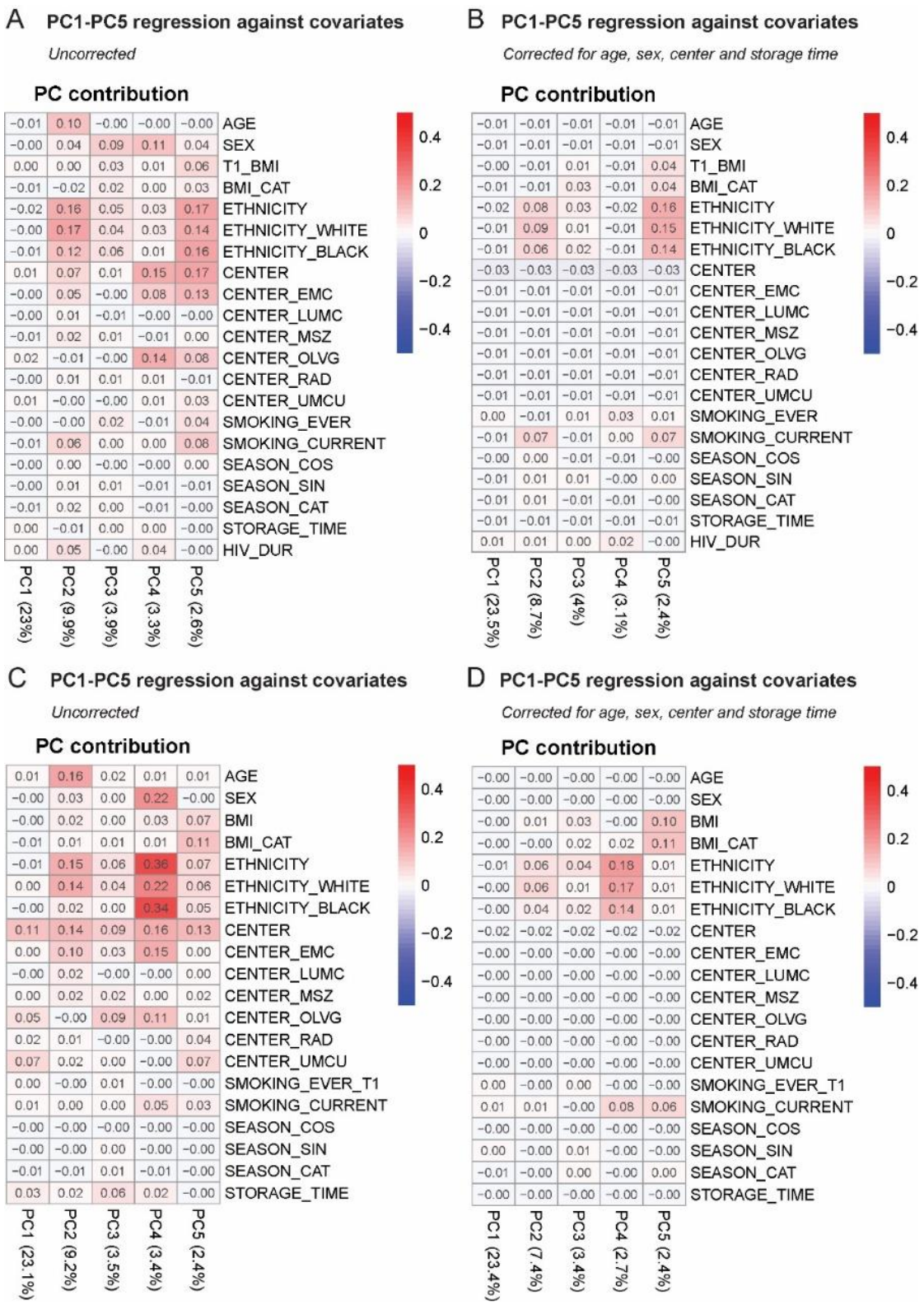

A,B,C,D. Heatmap depicting the associations between first 5 principal components (PCs) of proteomic data and list of possible confounders. The color-coding key depicts the beta estimate calculated by a linear regression model. A.B, include 183 individuals in the eliteATHENA study. C.D. include 288 paired samples for 144 individuals. A,D. show associations in the uncorrected data, whereas B,D. associations after correcting for age, sex, center and storage time.

Supplementary Figure 2 – Stratified analysis of potential confounders for the analysis in Figure 1

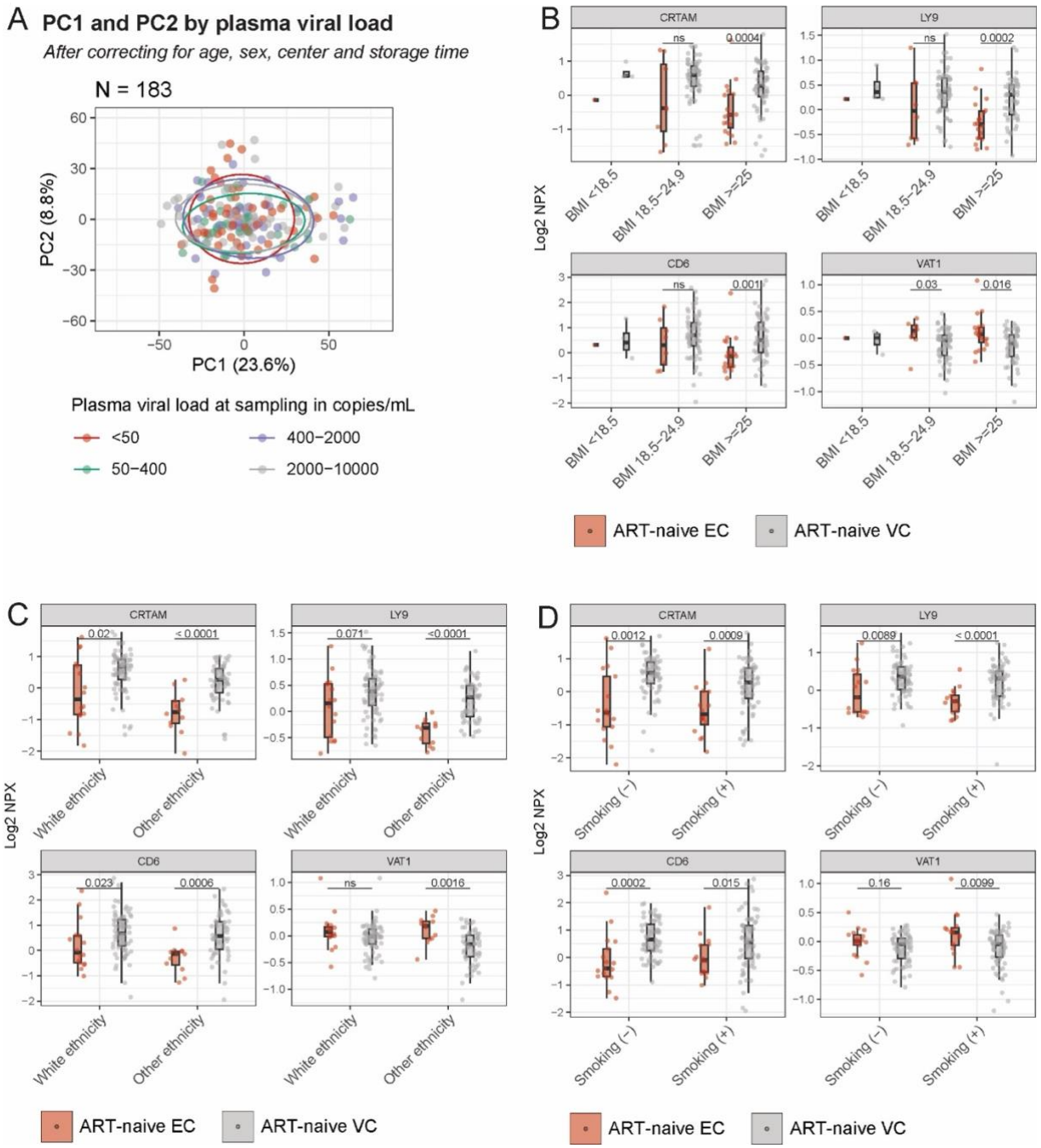

A. Principle component analysis graph of protein levels from the discovery cohort of different viral load cut-off using the first two principal components. The median differences of PC1 and PC2 between groups were assessed by the Wilcoxon test. All P-value were >0.05 (no significant differences were found). This analysis included 183 individuals in the eliteATHENA study.

B,C,D. Violin boxplot showing the comparison CRTAM, LY9, CD6, and VAT1 between persistent, ART naïve VC and EC stratified by smoking status, body mass index (BMI) and ethnicity of the discovery cohort (elite-ATHENA cohort). P values were derived from Wilcoxon test. In all boxplots, the in-box line defines the median value, hinges depict 25th and 75th percentiles and whiskers extend to 1.5 interquartile ranges; each dot indicates an individual participant.

Supplementary Figure 3 – Stratified analysis of the effect of ART and time on plasma proteomics

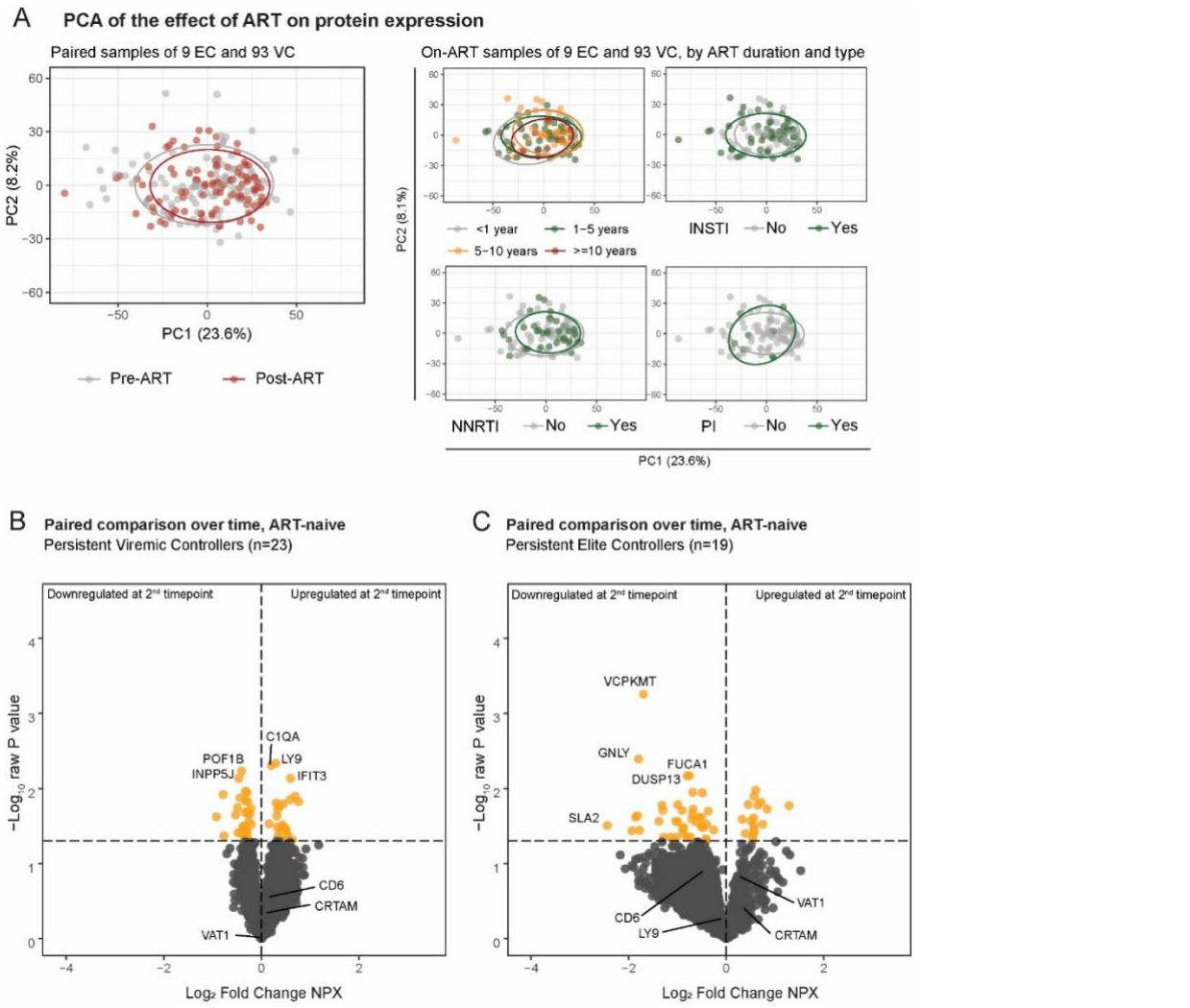

D Age-matched nested case-control differential protein expression before and after ART

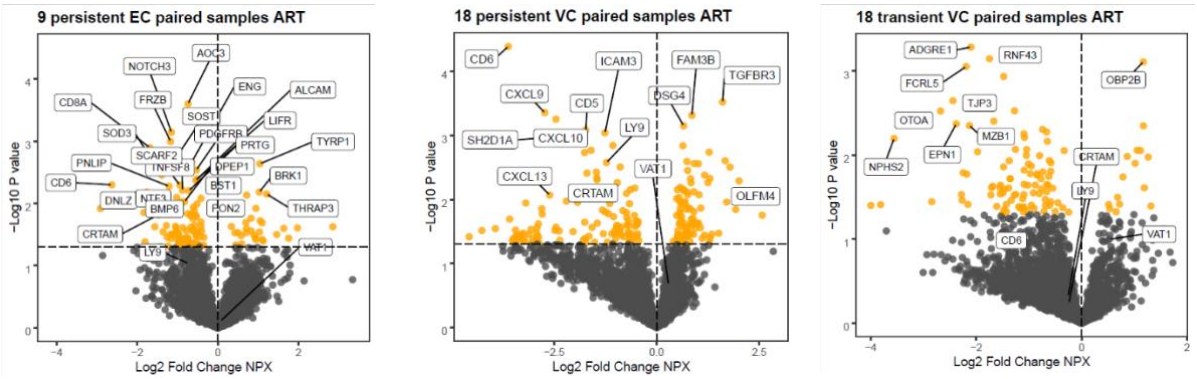

A. Principle component analysis plot of protein levels from the discovery cohort of HIV controllers before and after ART-medication (N=102 paired data of 9 EC and 93 VC) using the first two principal components. The median differences of PC1 and PC2 between groups were assessed by the Wilcoxon test. All P-value were >0.05.

B,C. Volcano plot of the differentially expressed proteins between paired participants on two different time points in (B) persistent VC (N=23), (C) persistent EC (N=19) in the discovery cohort. X-axis depicts Log2 fold change of differentially expressed proteins and Y-axis depicts -log10(P value). Differential expression analysis was performed using linear mixed models with age, sex, center and storage time as covariates. There were no FDR significant changes over time.

D. Volcano plots showing differentially expressed proteins between paired pre-ART and on-ART samples in age-matched persistent EC (N=9), persistent VC (N=18), and transient VC (N=18). X-axis depicts Log2 fold change of differentially expressed proteins and Y-axis depicts -log10(P value). Differential expression analysis was performed using linear mixed models with sex, center and storage time as covariates.

Supplementary Figure 4 – Relation between plasma viral load and CD4 T cell count trajectories and plasma proteomics.

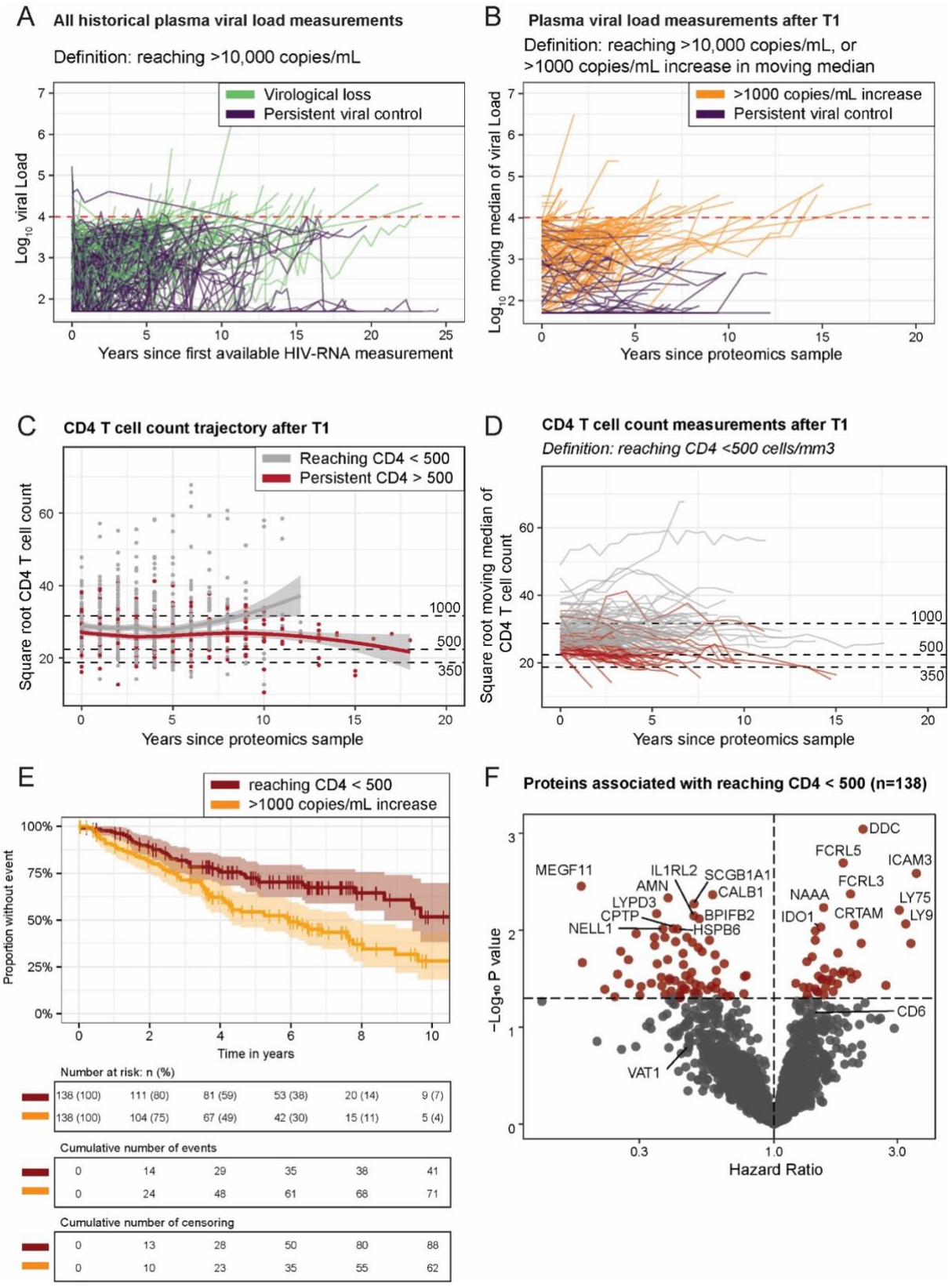

A. Line plot of all historical viral load measurements, including the ones before proteomics measurement between transient and persistent HIV controllers. Virological loss is defi ned as reaching > 10,000 copies/mL. Y axis depicts $\log_{10}$ viral load and X-axis depicts years since first HIV RNA measurement. This analysis includes 181 ART-naive HIV controllers (145 VC and 36 EC).
B. Line plot of follow-up viral load measurements after proteomics sample by substantial virus increase, defined as an increase of at least 1000 copies/mL in the moving median or reaching > 10,000 copies/mL. X-axis depicts years since first HIV RNA measurement and Y axis depicts the moving median of the viral load measurements on a $\log_{10}$ scale. The moving median takes into account all available viral load measurements in a span of -365 to +365 days. This analysis includes 181 ART-naive HIV controllers (145 VC and 36 EC).
C. Dot plot of all available historical $CD4^+$ T cell measurements between those reaching $CD4^+$ T cell counts < 500 cells/mm^3. Y axis depicts square root $CD4^+$ T cell count and X-axis depicts years since first HIV RNA measurement. The lines indicate the local regression (LOESS) fit; each dot represents an individual viral load measurement from one participant. This analysis includes individuals with available longitudinal CD4 data and CD4 counts >500 cells/mm^3 at the time of proteomics sample (N=138).
D. Line plot of follow-up $CD4^+$ T cell measurements after proteomics sample by immunological progression defined as reaching $CD4^+$ T cell < 500 cells/mm^3. For both **C** and **D**, data is only shown for N = 138 individuals with available longitudinal $CD4^+$ T cell data and $CD4^+$ T cell counts > 500 cells/mm^3 at the time of proteomics sample.
E. Kaplan-Meier loss-free follow-up. Vertical tick marks represent censored data points, indicating either end of follow-up or censoring by ART initiation in the absence of loss of virological control. The number at risk and cumulative number of events and censoring are reported. Substantial virus increase is defined as an increase of at least 1000 copies/mL in the moving median or reaching > 10,000 copies/mL. Immunological loss is defined as reaching $CD4^+$ T cell < 500 cells/mm^3. This is only shown for N = 138 individuals with available longitudinal $CD4^+$ T cell data and $CD4^+$ T cell counts > 500 cells/mm^3 at the time of proteomics sample.
F. Volcano plot of the differentially expressed proteins associated with immunological loss defined as reaching $CD4^+$ T cell < 500 cells/mm^3. X-axis depicts hazard ratio of differentially expressed proteins and Y-axis depicts $-\log_{10}$ (P value), where a hazard ratio > 1 means increased risk of immunological loss. Differential expression analysis was performed using cox regression with age, sex, center and storage time as covariates. This analysis includes individuals with available longitudinal CD4 data and CD4 counts >500 cells/mm^3 at the time of proteomics sample (N=138).

Supplementary Figure 5 – Machine learning models to predict future loss of control with clinical predictors

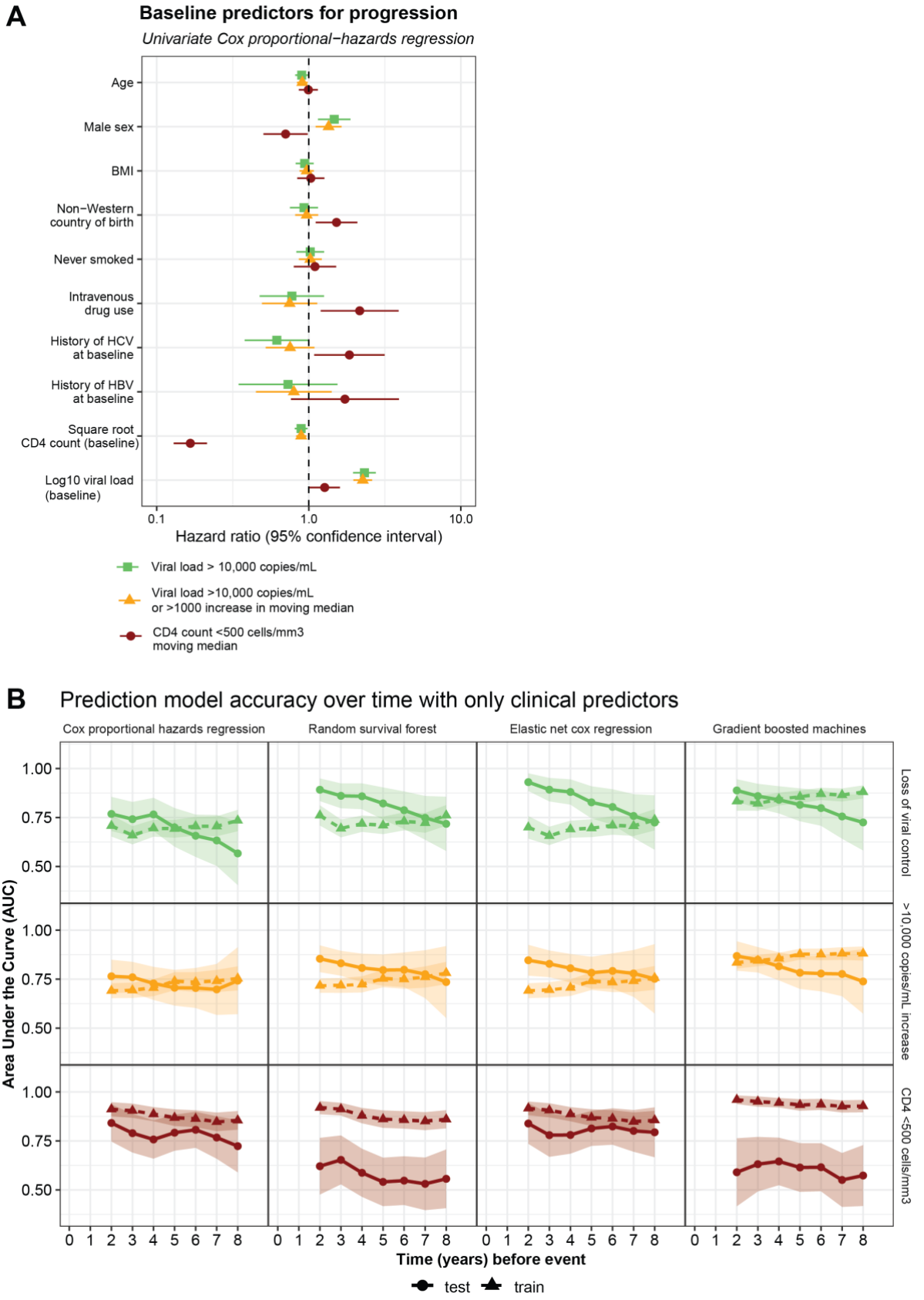

A. Associations between clinical baseline predictors and loss of viral control (> 10,000 copies/mL), substantial viral load increase (> 1000 copies/mL increase or reaching > 10,000 copies/ mL) or CD4 decline (reaching $CD4^+$ T cell count < 500 cells/mm^3) with 839 HIV controllers from the Dutch ATHENA cohort were assessed with univariate cox proportional hazard regression. BMI, body mass index in kg/m^2; HCV, hepatitis C virus; HBV, hepatitis B virus. A hazard ratio above 1 means presence of binary predictors is associated with earlier progression; or for continuous predictors, hazard ratio above 1 means that higher levels are associated with earlier progression.

B. Prediction model accuracy as assessed by area under the receiver operator curve (AUC) was calculated in predicting loss of viral control (> 10,000 copies/ mL), substantial viral load increase (> 1000 copies/mL increase or reaching > 10,000 copies/mL) or CD4 decline (reaching $CD4^+$ T cell count < 500 cells/mm^3), for yearly future timepoints. Models were trained with 839 HIV controllers from the Dutch ATHENA cohort and tested on 181 HIV controllers who had available proteomics data*. Triangles represent the accuracy for HIV controllers in the training dataset, circles the accuracy for HIV controllers in the testing dataset. *For CD4 decline, this was 565 and 138 HIV controllers as training and testing dataset, respectively.

Supplementary Figure 6 - Machine learning models to predict future loss of control with proteomics

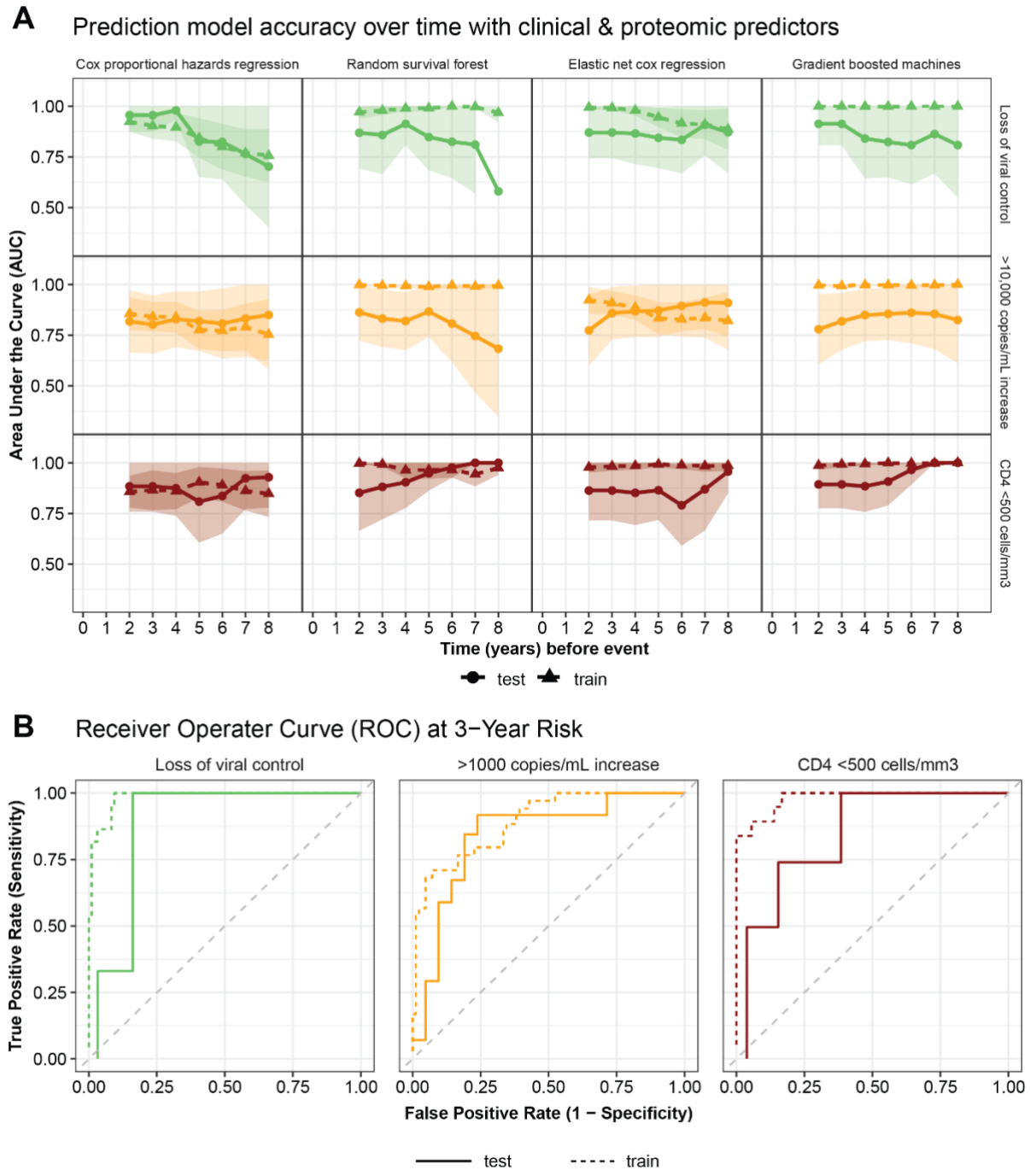

A. Prediction model accuracy as assessed by area under the receiver operator curve (AUC) was calculated in predicting loss of viral control (> 10,000 copies/mL), substantial viral load increase (> 1000 copies/mL increase or reaching > 10,000 copies/mL) or CD4 decline (reaching $CD4^+$ T cell count < 500 cells/mm^3), for yearly future timepoints. Models were trained with 134 HIV controllers (centers OLVG and EMC) and tested on 47 HIV controllers (centers UMCU, MSZ, RUMC, LUMC)*. Triangles represent the accuracy for HIV controllers in the training dataset, circles the accuracy for HIV controllers in the testing dataset.
B. To illustrate, prediction model accuracy is displayed for Elastic Net Cox Regression (Lasso) at predicting outcomes 3 years into the future with Receiver Operator Curves (ROC). Dashed and solid lines represent performance on the training and testing dataset, respectively. *For CD4 decline, this was 104 and 34 HIV controllers as training and testing dataset, respectively.

Supplementary Figure 7 – Relation between predictive proteins and inflammation, immune activation and residual viremia

A.

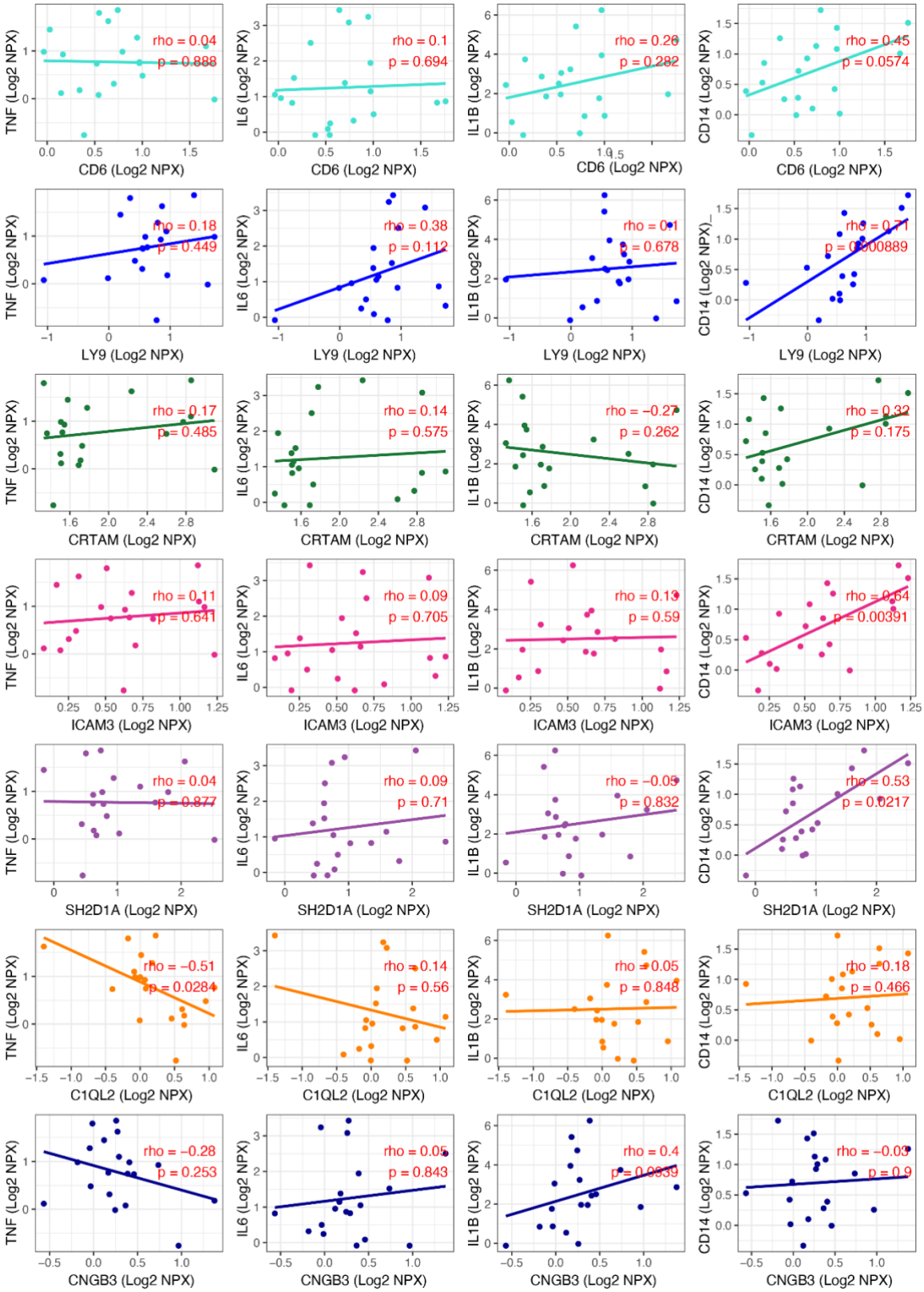

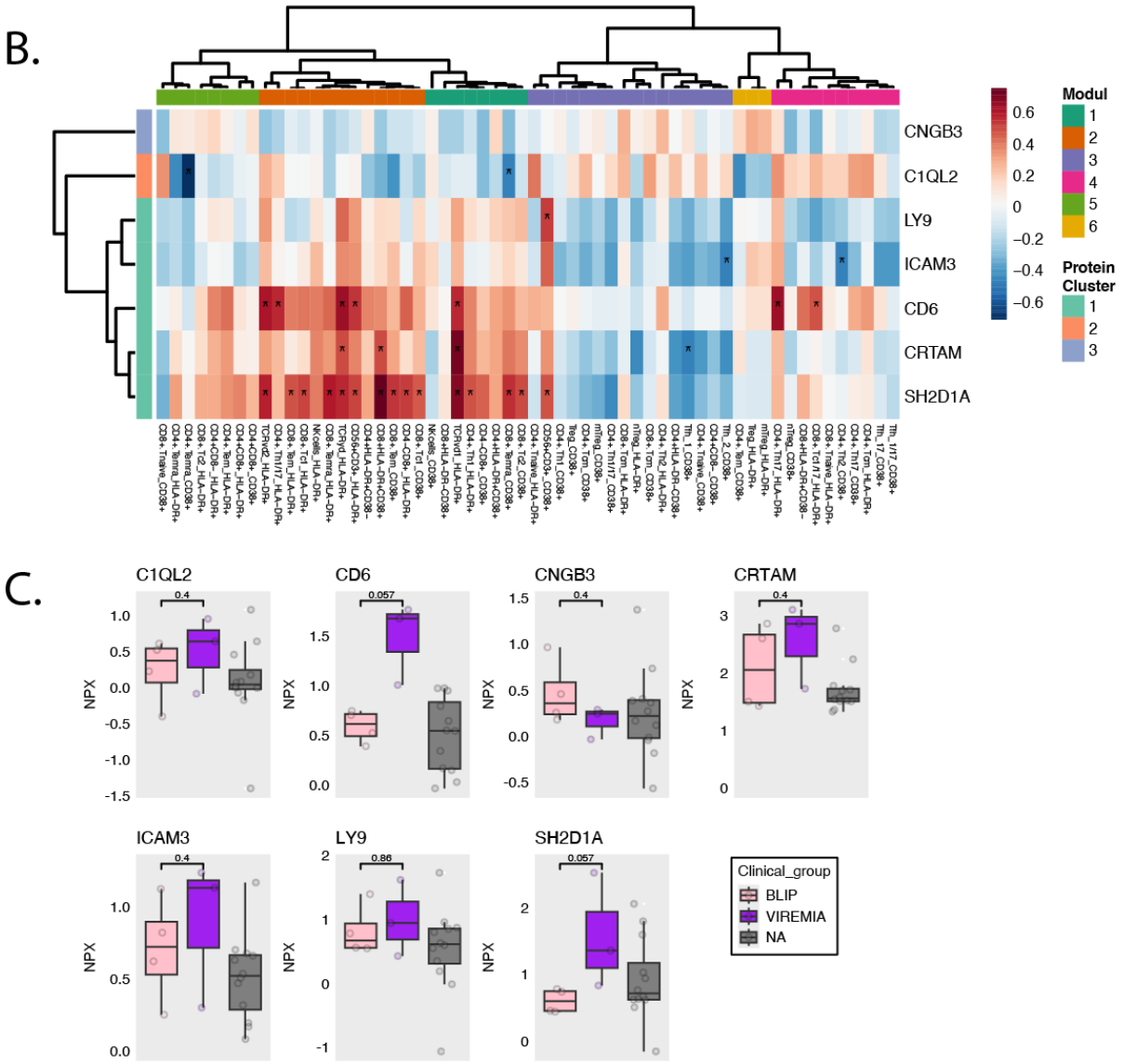

A. Scatterplots illustrate the associations between CRTAM, LY9, CD6, VAT1, ICAM3, SH2D1A, C1QL2, and CNGB3 on the one side, and established inflammatory markers (TNF, IL-6, IL-1β, and sCD14) (on the other side. Data derived from ART-naive HIV controllers (HIC) in the the 2000HIV cohort, including EC (N=14) and VC (N=5). Spearman correlation coefficients (rho) and corresponding P values are reported for each association. Both axes represent Log2 NPX values, and each point corresponds to a single participant.

B. Heatmap illustrates the Spearman correlations between seven proteins (CRTAM, LY9, CD6, ICAM3, SH2D1A, C1QL2, and CNGB3) and the absolute number of HLA-DR$^+$CD38$^+$ T-cell subsets. Data derived from ART-naive HIV controllers (HIC) in the 2000HIV cohort, including EC (N=14) and VC (N=5). Tiles are colored by rho value (red = positive, blue = negative), with hierarchical clustering (Ward's method on 1–|rho| distances) grouping proteins and cell subsets by similarity of their correlation profiles. Each tile displays an asterisk (*) if the correlation is significant (P value< 0.05). Each rho and P value reflects one protein–subset pairing across individual participants.

C. Boxplot comparing CRTAM, LY9, CD6, ICAM3, SH2D1A, C1QL2, and CNGB3 expression levels across three categories of quantifiable viral load over the last three years: viral blip (VL 40-200), viremia (VL 200-1000), and unknown, in ART-naive HIV controllers (HIC) from the 2000HIV cohort. The cohort includes EC (N=14) and VC (N=5). P values were derived from the Wilcoxon test. In all boxplots, the in-box line defines the median value, hinges depict 25th and 75th percentiles and whiskers extend to 1.5 interquartile ranges; each dot indicates an individual participant

Supplementary Figure 8 – Viral genome sequences of four viremic controllers

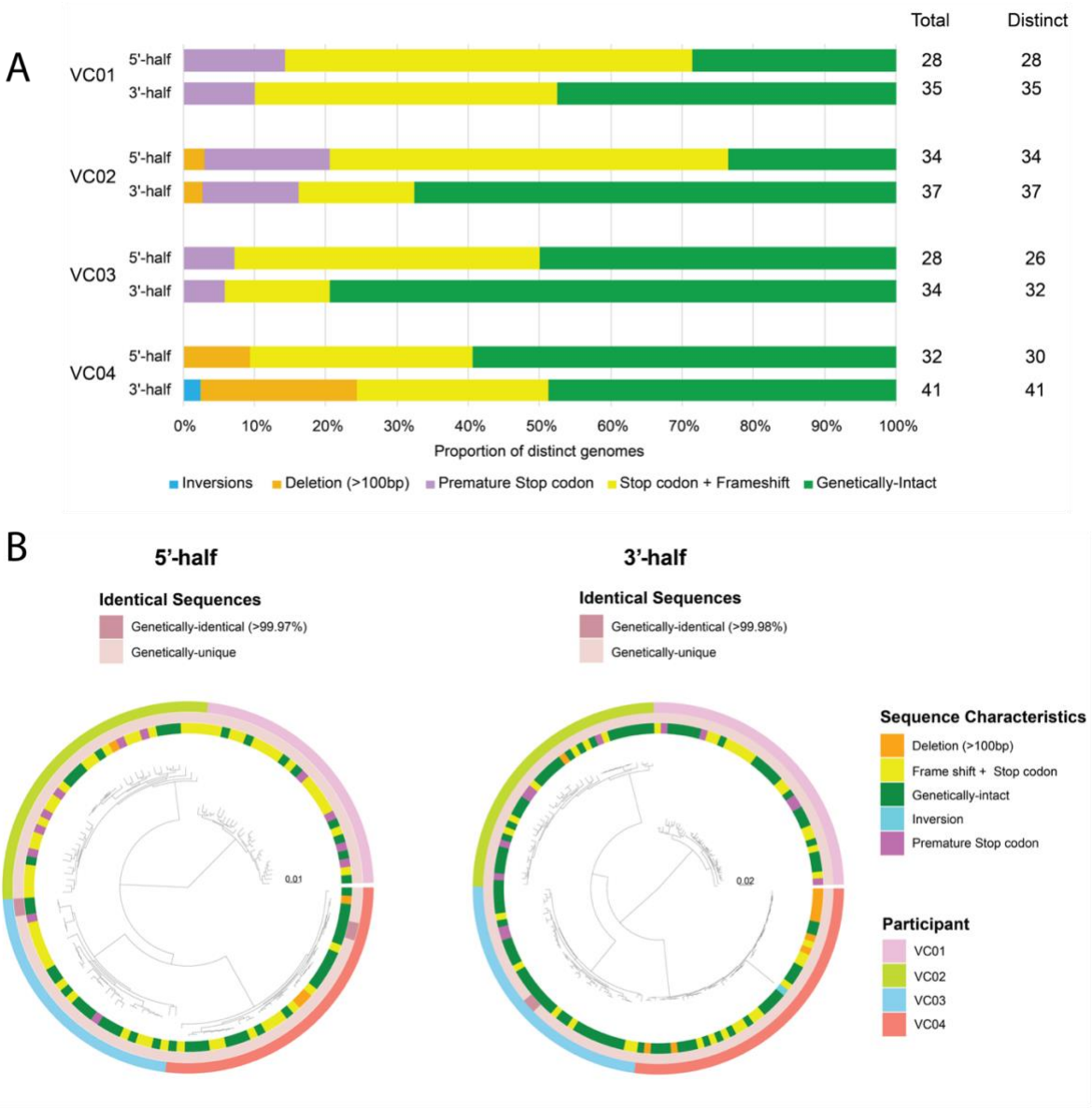

A. Plasma viruses as assayed by half-genome amplification assay. The proportions of different classes observed among the distinct plasma viruses for each participant (N=4 VC). On the right, a comprehensive display of total and distinct sequence counts is presented for each participant.

B. Phylogeny of plasma-derived sequences from 4 VC. Phylogenetic trees were prepared from the sequenced 5'-half and 3'-half-genomes. The outer rings of the trees display the participant IDs; the middle rings indicate whether the sequence shares more than 99.97% identity (for 5'-half) or 99.98% identity (for 3'-half) with another sequence in the tree; and the inner rings display the classification of sequences as genetically-intact or defective within the sequenced region, with specific types of defects depicted.